Additive manufacturing of micro-architected copper based on an ion-exchangeable hydrogel

Songhua Ma[a], Wuxin Bai[a], Dajun Xiong[a], Guibin Shan[d], Zijie Zhao*[c], Wenbin Yi*[a], Jieping Wang*[a],[b]

[a] S. Ma, W. Bai, D. Xiong, W. Yi, J. Wang
School of Chemistry and Chemical Engineering, Nanjing University of Science and Technology
Nanjing University of Science and Technology
Nanjing 210094, China
E-mail: yiwb@njust.edu.cn; jieping.wang@njust.edu.cn

[b] J. Wang
State Key Laboratory of Powder Metallurgy
Central South University
Changsha 410083, China

[c] Z. Zhao
National Key Laboratory of Transient Physics
Nanjing University of Science and Technology
Nanjing 210094, China
Email: zj.zhao@njust.edu.cn

[d] G. Shan
Herbert Gleiter Institute of Nanoscience, School of Material Science and Engineering
Nanjing University of Science and Technology
Nanjing 210094, China

Supporting information for this article is given via a link at the end of the document.

Abstract: Additive manufacturing (AM) of copper through laser-based processes poses challenges, primarily attributed to the high thermal conductivity and low laser absorptivity of copper powder or wire as the feedstock. Although the use of copper salts in vat photopolymerization-based AM techniques has garnered recent attention, achieving micro-architected copper with high conductivity and density has remained elusive. In this study, we present a facile and efficient process to create complex 3D micro-architected copper structures with superior electrical conductivity and hardness. The process entails the formulation of an ion-exchangeable photoresin, followed by the utilization of digital light processing (DLP) printing to sculpt 3D hydrogel scaffolds, which were transformed into Cu^{2+}-chelated polymer frameworks (**Cu-CPFs**) with a high loading of Cu^{2+} ions through ion exchange, followed by debinding and sintering, results in the transformation of **Cu-CPFs** into miniaturized copper architectures. This methodology represents an efficient pathway for the creation of intricate micro-architected 3D metal structures.

Copper assumes a pivotal role in the fabrication of essential components across diverse domains, encompassing aerospace[1], nanotechnology[2], thermodynamic engineering[3], and medical industry[4]. This is attributed to its exceptional thermal (401 W/(m·K)), electrical conductivity (1.68 μΩ·cm) and scalability, along with its antibacterial properties[5-6]. The utilization of additive manufacturing (AM) techniques facilitates the creation of intricate copper geometries, thereby enabling innovative designs that were previously considered impractical or unattainable through conventional manufacturing methods. Techniques such as selective laser melting (SLM)[7], powder bed fusion (PBF)[8], electron beam additive manufacturing (EBAM)[9], low reflectivity metal coating[10], binder jetting[11], and ultrasonic additive manufacturing (UAM)[12] have been specifically developed for copper AM, employing either copper powder or wire as the primary feedstock. However, the notable thermal conductivity of copper poses challenges in terms of heat dissipation from the melt areas during the AM process. This can lead to issues such as warping, cracking, or inconsistent layer bonding. Additionally, the formation of an oxide layer on copper surfaces can adversely impact the quality of printed parts, necessitating precise control over the printing environment and process parameters[13].

The recent exploration of utilizing metal salts for metal AM has gained traction. Electrochemical deposition is employed to generate metal microstructures by directing metal salts through an electric field and redox reactions. However, its application is constrained by limited design flexibility and a restricted manufacturing scale[14-15]. The integration of metal salts into vat polymerization has successfully addressed the resolution challenge associated with the size of raw materials and has overcome constraints linked to materials reliant on thermal initiation[16-20]. Nevertheless, the direct incorporation of copper salts into photoresins as a physical dopant may induce particle refraction and physical sedimentation during the photocuring process[21-22]. Furthermore, the presence of Cu^{2+} may hinder free radical polymerization[23], resulting in low conductivity and resolution limitations[24]. Greer et al. introduced a hydrogel infusion additive manufacturing (**HIAM**)[5] technique, where

copper microstructures were fabricated by utilizing hydrogels to absorb Cu^{2+} through multiple processes. However, the introduction of metal ions could significantly impact the water absorption capacity of the hydrogel[25], leading to limited Cu^{2+} loading (9.90 wt%) and resulting in defects such as layered cracks in the subsequent sintered samples.

Herein, we present a facile and robust strategy for the creation of complex and dense micro-architected copper with elevated conductivity and hardness (Figure 1a). The process involves the utilization of a water-based photoresin containing ion-exchangeable monomers, enabling the sculpting of 3D hydrogel scaffolds via DLP. Subsequent immersion of these scaffolds in a $CuSO_4$ solution results in a notable high loading of Cu^{2+} ions (20.31 wt%) achieved through ion exchange. Following debinding in air and sintering in a reducing atmosphere, the resulting copper architectures exhibit a minimum feature size of approximately 40 μm, accompanied by a high twin density and substantial copper content (96.2 wt%). The microstructure of copper is microcrystalline and compact, featuring an average grain size of 6.5 μm and 4.6 ± 2.2 twins per grain. These findings underscore the powerful capability of this methodology in creating micro-architected 3D metal structures.

A water-based photoresin was developed, comprising sodium acrylate as an ion-exchangeable monomer, polyethylene glycol diacrylate (PEGDA) as a crosslinker, PEG-BAPO[26] as a highly efficient waterborne photoinitiator, tartrazine as a photo-blocker to fine-tune printing resolution[27], and cellulose nanocrystals (CNCs) as a toughening agent[28] (Figure 1b). Sodium acrylate was chosen as a key active ingredient, with Na^+ ions being replaced by Cu^{2+} ions due to their strong coordination[29]. Rheological measurements indicated that the incorporation of CNCs maintains a low resin viscosity, preserving the delay time while concurrently enhancing the elastic modulus after curing (Figure S1). Through the adjustment and optimization of printing parameters (Table S1), the successful fabrication of hydrogel scaffolds with a remarkable degree of design freedom was achieved. The addition of CNCs resulted in a reduction of the

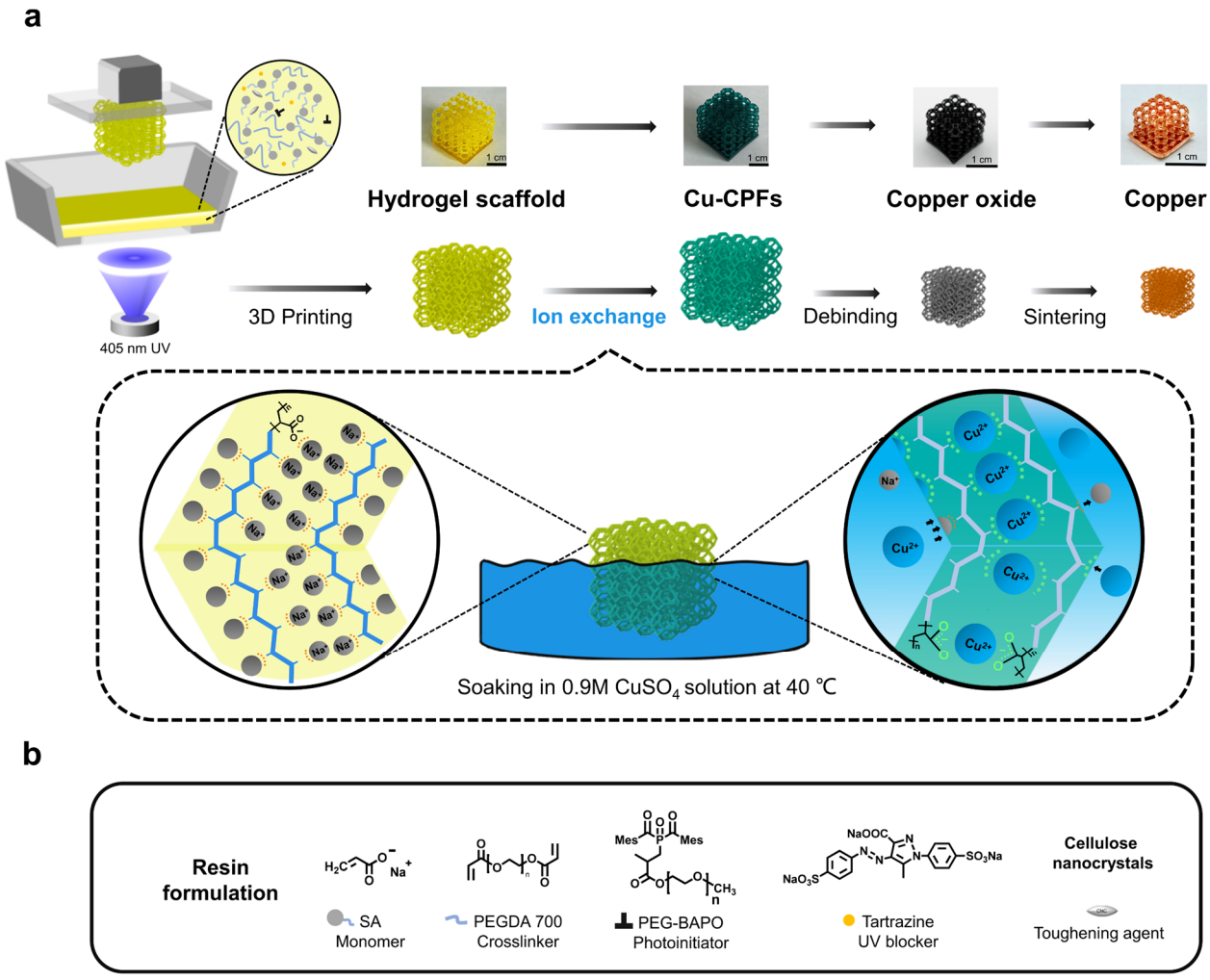

Figure 1. An overview of AM of micro-architected copper via ion exchange. a) Schematic illustration of the copper AM strategy. b) Resin formulation.

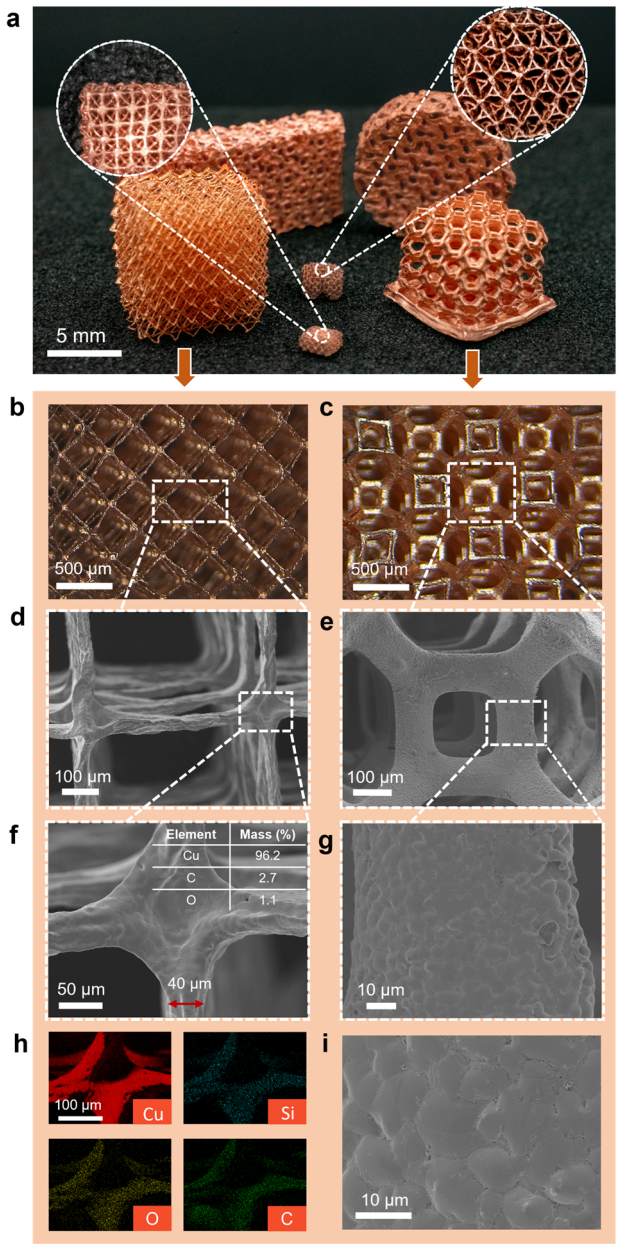

Figure 2. Morphology and composition analysis of copper structures. a) Multiscale copper complex structures with critical dimensions from 40-300 µm. b-g) Optical and scanning electron microscope (SEM) images of 3D printed copper. f) Octahedral structure with a critical dimension of 40 µm. Inset: EDS analysis of sintered 3D printed copper. h) EDS element maps showing the homogenous distribution of copper (the darker area is a result of surface irregularities present in the sample). i) SEM images of the surface morphology of 3D printed copper.

minimum feature size from 300 µm to 80-100 µm (Figure S2).

Subsequently, the scaffolds underwent immersion in a $CuSO_4$ solution, followed by rinsing to eliminate water-soluble impurities and surface-adsorbed copper ions. The concentration of $CuSO_4$, immersion temperature, and duration emerged as crucial factors in the ion exchange process, intricately linked to model fidelity and Cu^{2+} loading. Observing the structural fidelity of the resulting Cu^{2+}-chelated polymer frameworks (**Cu-CPFs**), we determined the optimal $CuSO_4$ solution concentration to be 0.9M (Figure S3c). It is acknowledged that an increase in immersion temperature accelerates the ion exchange rate, thereby enhancing Cu^{2+} permeability. However, excessively high temperatures exert an overly dominant penetration force during the initial stages, potentially leading to rupture and deformation of hydrogel scaffolds that have not undergone sufficient ion exchange (Figure S3e-h). Through incremental adjustments in immersion temperature, we identified 40°C as the optimal temperature, considering fidelity and the internal immersion depth of the **Cu-CPFs**, determined through physical sectioning. Complemented by the suitable immersion temperature, the duration was set at 3-7 days, depending on the critical size of the structures. The maximum thickness of **Cu-CPFs** with a uniform solid interior reached up to 6mm (Figure S4). Ultimately, densely packed (Figure S5) and high-fidelity **Cu-CPFs** were realized. The successful coordination of Cu^{2+} was confirmed via ATR-FTIR, where the stretching vibration of the carbonyl ($\nu_{c=o}$) at 1545 cm^{-1} within the hydrogel shifted to a higher wavenumber at 1616 cm^{-1} in **Cu-CPFs** (Figure S6). The Cu^{2+} loading capacity (20.31 wt%, Figure S7, Note S1), closely approaching the theoretical value (23.11 wt%, Note S1), surpassed that of the **HIAM** technique by a factor of two. This positions our approach as a competitive alternative to metal fabrication via vat polymerization, involving direct doping of metal salts and the incorporation of hybrid organic–inorganic materials (Figure S8).

The debinding and sintering parameters of **Cu-CPFs** underwent systematic investigation to attain optimal copper structural characteristics. In contrast to the physical doping of conventional methods, we noted that the objects exhibited bulging during the debinding stage when the heating rate was excessively slow. This phenomenon revealed the presence of a carbon coating on the surface, highlighting issues related to the subsequent release of pyrolysis gases (Figure S9). To address this challenge, we devised a thermal debinding heating scheme, optimizing it based on thermogravimetric analysis (TGA) data (Figure S7). The heating rate was regulated to maintain a controlled increase, limited to 1°C/min up to 450°C to prevent the formation of a carbon film. Additionally, the heating rate was reduced within a ±15°C range around specific temperatures (235°C, 315°C, and 385°C) to establish platform periods (Figure S10a). The resulting copper oxide exhibited high purity, confirmed by X-ray diffraction (XRD) (Figure S11a) and energy dispersive X-ray spectroscopy (EDX) analysis (Figure S12). The microstructure of the copper oxide manifested a porous appearance with particle diameters of approximately 100 nm. Scanning electron microscopy (SEM) revealed that a slow sintering heating rate led to a lower surface density (Figure S13), while a brief reduction time resulted in sintered samples retaining unreduced copper oxide (Figure S14). Consequently, the sintering procedure was established with a heating rate of 3°C/min, ascending to 900°C, and maintained at this temperature for 1000 minutes (Figure S11b).

Subsequently, intricate copper architectures spanning from submillimeter to centimeter scales, exhibiting high fidelity and density (Figure S15), were successfully obtained (Figure 2a). The uniform distribution of Cu^{2+} within **Cu-CPFs** led to an isotropic shrinkage of approximately 60% (Figure S16) in the final

structures. The achieved minimal feature size is 40 μm (Figure 2f), surpassing the commonly encountered constraint in most copper AM, which limits precision to levels above 100μm (Figure S17 and Table S3). EDX analysis revealed that the sintered parts contained 96.2 wt% copper, 2.7 wt% carbon, and 1.1 wt% oxygen (Figure 2h), with incidental surface contamination of silicates from the furnace tube (Figure S19). Furthermore, SEM analysis confirmed the retention of structural integrity and related properties in the fabrication of copper structures with larger feature sizes (Figure 2g, i). A remarkable achievement in integrated copper AM is highlighted by the achieved resistivity as low as 4.91 μΩ·cm (equivalent to 2.9 times that of bulk copper), accomplished without utilizing heat pressing or deposition (Figure S20 and Table S4). This underscores the establishment of a consistent and enduring electric field, emphasizing the high density and excellent electrical conductivity inherent in the fabricated structures (Figure S21).

The sintered copper, exhibiting a random orientation, is rich in special microstructures (Figure S22), notably annealed twins as confirmed by the selected area electron diffraction (SAED) patterns (Figure 3a, b). The twin boundary was further verified using high-resolution transmission electron microscopy (HRTEM) (Figure 3c). A fast Fourier transform (FFT) of the entire image highlights the double-spot characteristic indicative of twinning (the inset in Figure 3c). Additionally, electron backscatter diffraction (EBSD) mapping illustrates the presence of copper with a high-volume fraction of twins (Figure 3d). Nanoindentation measurements unveiled a notable hardness value for the copper, reaching 1.72 ± 0.22 GPa (Figure S23). Notably, this hardness value surpasses expectations based on the Hall-Petch curve

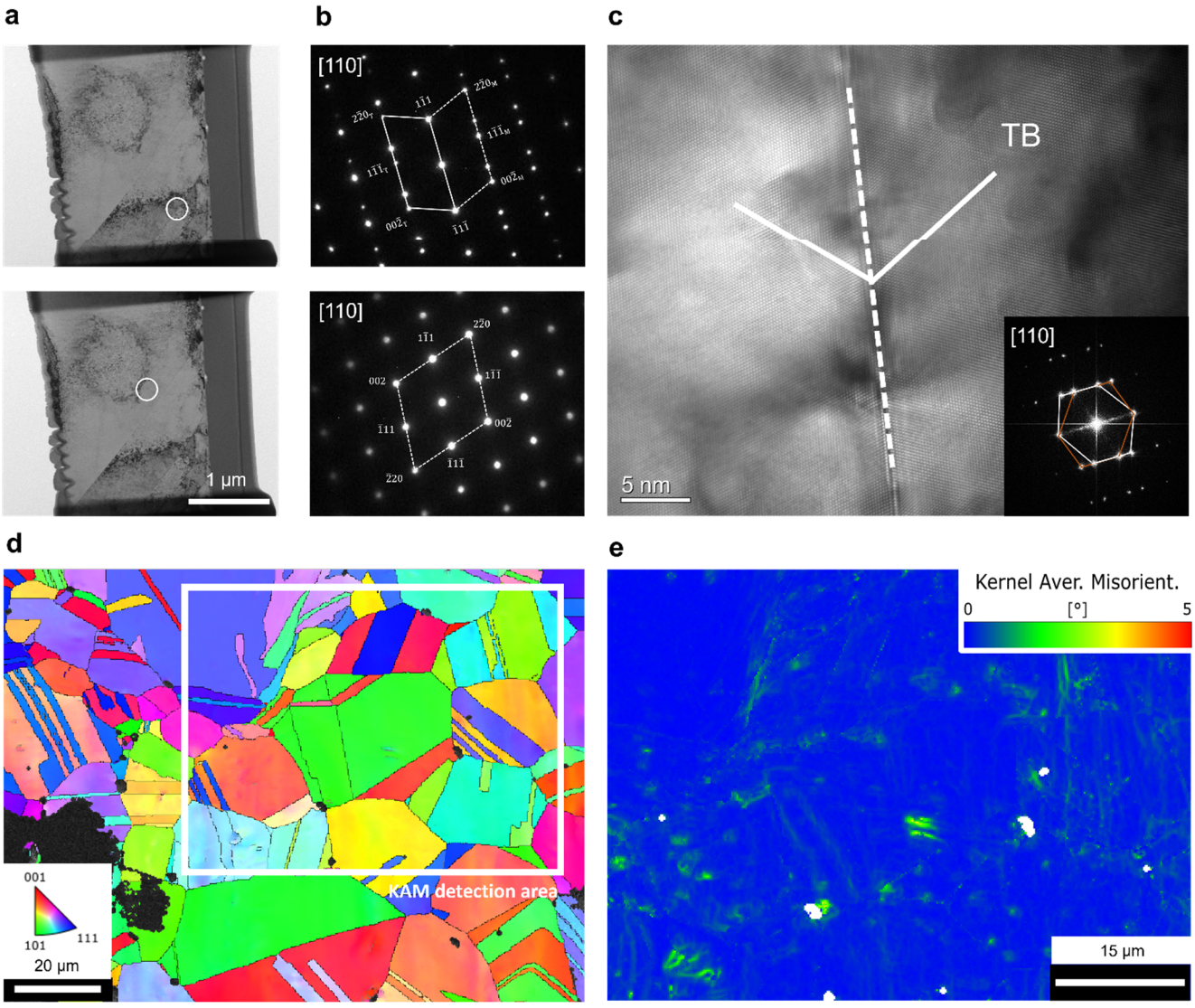

Figure 3. Characterizations of annealing twin microstructures and mechanical properties. a) TEM images of FIB-ed samples. b) SAED patterns corresponding to the region of the white circle in b. c) An HRTEM image of Cu showing a coherent twin boundary. Dashed lines indicate the twin boundary (TB), and mirrored solid lines indicate the lattice directions on both sides of TBs. The inset shows the FFT of the whole image, showing the double-spot characteristic of twinning. d) EBSD map of Cu. e) EBSD-KAM images of 3D-printed Cu.

(Table S8)[30-32]. This may be attributed to residual light atoms (e.g., carbon, oxygen) dissolved into the lattice or at the grain boundaries, acting as obstacles for dislocation motion[5, 33], along with the roughness of grain boundaries caused by grain growth and interlocking upon reduction[34]. To showcase the macro mechanical properties of the 3D-printed Cu, quasi-static compression experiments were conducted on the printed Cu architecture and commercial copper foam (Figure S25a). The compressive strength of the Cu architecture (10.3 MPa) significantly exceeded that of commercial copper foams (1.7 MPa). The Cu architecture yielded 40% compressive stress, attributed to the well-ordered structure effectively dispersing the force (Figure S25b) and the contribution of crystallites and twins hindering dislocations.

To conclude, we have successfully established a facile and efficient process for creating micro-architected copper through the utilization of an ion-exchangeable hydrogel. This method's inherent exceptional copper ion loading capacity, combined with its indirect printing approach free from model limitations, enables the fabrication of intricate multi-scale copper structures with remarkable electrical conductivity and hardness. This breakthrough holds significant potential for advancing various fields, including electrochemical energy systems, micro-electromechanical systems, and catalysis. The method's inherent ion-exchange properties, unrestricted by resin limitations, could pave the way for future applications with various metals, opening new avenues for exploration and innovation in material fabrication.

Supporting Information

The authors have cited additional references within the Supporting Information.

Acknowledgements

We thank Prof. Jinfeng Nie, Prof. Xiang Chen, and Prof. Bingqing Xu, all from Nanjing University of Science and Technology, and Prof. Chao Chen, from Central South University, for fruitful discussions and proofreading of the manuscript. We gratefully acknowledge the National Natural Science Foundation of China (52103217, 22078161), the Fundamental Research Funds for the Central Universities (30920021124, 30918011314, 30921011205), the High-level personnel project of Jiangsu Province (JSSCBS20210227) for their financial support. J.W. also acknowledges the strong support provided by the State Key Laboratory of Powder Metallurgy, Central South University, Changsha, China.

Keywords: additive manufacturing, photopolymerization, copper, hydrogel, ion exchange

[1] A. Marques, B. Guimarães, M. Cerqueira, F. Silva, O. Carvalho, *Adv. Eng. Mater.* **2022**, *25*, 2201349.
[2] Y. Jo, H. J. Park, Y. B. Kim, S. S. Lee, S. Y. Lee, S. K. Kim, Y. Choi, S. Jeong, *Adv. Funct. Mater.* **2020**, *30*, 2004659.
[3] F. Singer, D. Deisenroth, D. Hymas, M. Ohadi, in *2017 16th IEEE Intersociety Conference on Thermal and Thermomechanical Phenomena in Electronic Systems (ITherm)*, IEEE, **2017**, pp. 174-183.
[4] E. Gutierrez, P. A. Burdiles, F. Quero, P. Palma, F. Olate-Moya, H. Palza, Engineering, *ACS Biomater. Sci. Eng.* **2019**, *5*, 6290-6299.
[5] M. A. Saccone, R. A. Gallivan, K. Narita, D. W. Yee, J. R. Greer, *Nature* **2022**, *612*, 685-690.
[6] L. Constantin, Z. Wu, N. Li, L. Fan, J.-F. Silvain, Y. F. Lu, *Addit. Manuf.* **2020**, *35*, 101268.
[7] S. D. Jadhav, S. Dadbakhsh, L. Goossens, J. P. Kruth, J. Van Humbeeck, K. Vanmeensel, *J. Mater. Process Technol.* **2019**, *270*, 47-58.
[8] W. E. King, A. T. Anderson, R. M. Ferencz, N. E. Hodge, C. Kamath, S. A. Khairallah, A. M. Rubenchik, *Appl. Phys. Rev.* **2015**, *2*, 041304.
[9] C. Silbernagel, L. Gargalis, I. Ashcroft, R. Hague, M. Galea, P. Dickens, *Addit. Manuf.* **2019**, *29*, 100831.
[10] S. Wong Kam, M. Yan, R. Gu, *Sci. China- Phys. Mech. Astron.* **2019**, *50*, 034204.
[11] H. Miyanaji, D. Ma, M. A. Atwater, K. A. Darling, V. H. Hammond, C. B. Williams, *Addit. Manuf.* **2020**, *32*, 100960.
[12] D. Li, *Int. J. Adv. Manuf. Technol.* **2021**, *113*, 1-19.
[13] C. Ledford, C. Rock, P. Carriere, P. Frigola, D. Gamzina, T. Horn, *Appl. Sci.* **2019**, *9*, 3993.
[14] J. Hu, M. F. Yu, *Science* **2010**, *329*, 313-316.
[15] C. van Nisselroy, C. Shen, T. Zambelli, D. Momotenko, *Addit. Manuf.* **2022**, *53*, 102718.
[16] A. Vyatskikh, S. Delalande, A. Kudo, X. Zhang, C. M. Portela, J. R. Greer, *Nat. Commun.* **2018**, *9*, 593.
[17] M. Luitz, M. Lunzer, A. Goralczyk, M. Mader, S. Bhagwat, A. Warmbold, D. Helmer, F. Kotz, B. E. Rapp, *Adv. Mater.* **2021**, *33*, e2101992.
[18] D. W. Yee, M. L. Lifson, B. W. Edwards, J. R. Greer, *Adv. Mater.* **2019**, *31*, e1901345.
[19] I. Cooperstein, S. Indukuri, A. Bouketov, U. Levy, S. Magdassi, *Adv. Mater.* **2020**, *32*, e2001675.
[20] D. W. Yee, M. A. Citrin, Z. W. Taylor, M. A. Saccone, V. L. Tovmasyan, J. R. Greer, *Adv. Mater. Technol.* **2021**, *6*, 2000791.
[21] J. W. Halloran, *Annu. Rev. Mater. Res.* **2016**, *46*, 19-40.
[22] H. X. Nguyen, H. Suen, B. Poudel, P. Kwon, H. Chung, *CIRP Ann. Manuf. Technol.* **2020**, *69*, 177-180.
[23] J. Y. Hu, D. Jiao, X. P. Hao, X. Kong, X. N. Zhang, M. Du, Q. Zheng, Z. L. Wu, *Adv. Funct. Mater.* **2023**, 2307402.
[24] Y. Li, C. Li, X. Zhang, Y. Wang, Y. Tan, S. Chang, Z. Chen, G. Fu, Z. Kou, A. Stefan, X. Xu, J. Ding, *Appl. Mater. Today* **2022**, *29*, 101553.
[25] I. Katime, E. Rodríguez, *J. Macromol. Sci., Part A: Pure Appl. Chem.* **2001**, *38*, 543-558.
[26] J. Wang, S. Stanic, A. A. Altun, M. Schwentenwein, K. Dietliker, L. Jin, J. Stampfl, S. Baudis, R. Liska, H. Grutzmacher, *Chem. Commun.* **2018**, *54*, 920-923.
[27] M. Caprioli, I. Roppolo, A. Chiappone, L. Larush, C. F. Pirri, S. Magdassi, *Nat. Commun.* **2021**, *12*, 2462.
[28] J. Wang, A. Chiappone, I. Roppolo, F. Shao, E. Fantino, M. Lorusso, D. Rentsch, K. Dietliker, C. F. Pirri, H. Grutzmacher, *Angew. Chem. Int. Ed.* **2018**, *57*, 2353-2356.
[29] C. Dong, H. Fan, F. Tang, X. Gao, K. Feng, J. Wang, Z. Jin, *J. Mater. Chem. B* **2021**, *9*, 373-380.
[30] S. Bansal, E. Toimil-Molares, A. Saxena, R. R. Tummala, in *Proceedings Electronic Components and Technology, 2005. ECTC'05.*, IEEE, **2005**, pp. 71-76.
[31] F. Emeis, M. Peterlechner, S. V. Divinski, G. Wilde, *Acta Mater.* **2018**, *150*, 262-272.
[32] S.-Y. Chang, T.-K. Chang, *J. Appl. Phys.* **2007**, *101*, 033507.
[33] J. Guo, M. J. Duarte, Y. Zhang, A. Bachmaier, C. Gammer, G. Dehm, R. Pippan, Z. Zhang, *Acta Mater.* **2019**, *166*, 281-293.
[34] W. Zhang, Z. Li, R. Dang, T. T. Tran, R. A. Gallivan, H. Gao, J. R. Greer, *Nano Lett.* **2023**, *23*, 8162-8170.